Electrochimica Acta 209 (2016) 682–690

Contents lists available at ScienceDirect

Electrochimica Acta

journal homepage: www.elsevier.com/locate/electacta

Humidity and Temperature Dependences of Oxygen Transport Resistance of Nafion Thin Film on Platinum Electrode

Kenji Kudo*, Ryosuke Jinnouchi, Yu Morimoto

Toyota Central Research & Development Laboratories, Inc., Nagakute, Aichi, 480-1192, Japan

ARTICLE INFO

Article history:
Received 15 January 2016
Received in revised form 4 April 2016
Accepted 5 April 2016
Available online 14 May 2016

Keywords:
polymer electrolyte fuel cells
thin film
Nafion
ionomer
oxygen transport

ABSTRACT

The oxygen transport resistances of Nafion thin films on a Pt electrode and of a bulk Nafion were evaluated to clarify the dominant part of the oxygen transport loss in an ionomer for a cathode catalyst layer of polymer electrolyte fuel cells. To evaluate the oxygen transport resistances of the Nafion thin film, an oxygen flux through the Nafion thin film on the Pt was detected as diffusion limited current density, j_d, for an oxygen reduction reaction by using an electrochemical cell equipped with a Pt microelectrode coated with a Nafion film less than 100 nm. An interfacial oxygen transport resistance and inner resistivity of the Nafion thin film were separately determined by the relation between j_d^{-1} normalized by oxygen partial pressure and the film thickness. The interfacial resistance is equivalent to 30–70 nm of the Nafion film, which are much thicker than a typical ionomer thickness of ~10 nm observed in catalyst layers. From the above results and our recent theoretical results obtained by molecular dynamics techniques, the oxygen permeation fluxes through the ionomers in catalyst layers can be regarded as dominantly controlled by the oxygen permeation at the Pt/ionomer interface.

1. Introduction

Polymer electrolyte fuel cells (PEFCs) are clean power sources applicable to automobiles and residential co-generation systems. For their wide distributions, however, their cost needs to be reduced. Platinum electrocatalyst used at both the anode and cathode is one of the most expensive components in PEFCs [1], and therefore, its loading is desired to be reduced. For reducing the Pt loading without sacrificing the energy conversion efficiency, the catalytic activity for oxygen reduction reaction (ORR) at the cathode side of PEFCs needs to be enhanced, and for achieving that target, various types of advanced cathode electrocatalysts have been developed [2–9]. Recent studies, however, indicated that improving the mass-activity for ORR is not enough to achieve the decrease in Pt loading [10–17]. Greszler et al. [14], reported that when the Pt loading in membrane electrode assemblies (MEAs) is reduced down to a certain level, the voltage starts to drop in the high current density and mass-transport-control region. Similar drops were reported also by other research groups [12,15–17], and they were attributed to oxygen transport resistances near Pt catalyst surfaces in the cathode catalyst layers, contributions of which are increased when local oxygen fluxes are increased by the reduction in the Pt surface area (loading). The origin of the oxygen transport resistance, however, was not clarified by MEA experiments.

For clarifying the origin, our group adopted a model experiment using Nafion ionomer thin films coated on Pt planar electrodes [18–20]. This model experiment indicated that the high oxygen transport resistance near the Pt electrodes stems from the interfacial resistance at ionomer/Pt interfaces and/or gas/ionomer interfaces. This experimentally obtained suggestion was recently supported by a theoretical study using molecular dynamics simulations [21] which showed that oxygen permeations through the ionomer thin films are limited by permeations through dense ionomer layers formed at ionomer/Pt interfaces.

The interfacial resistance (1700–10000 s m^{-1}) measured by the model experiment [19] is, however, much larger than that (1000–2000 s m^{-1}) measured by MEAs [12,14]. This discrepancy can stem from the thickness difference of Nafion ionomer: 200–800 nm used in the model experiment and 10 nm or less in MEAs. Other model experimental studies carried out recently on Nafion thin films exhibited that thinner ionomer film have different properties in the proton conductivity, water absorptivity and macroscopic morphology from the bulky material [22–45]. Detailed experimental analysis indicated that those changes can be attributed to the confinement effects and/or the substrate-

* Corresponding author. Tel.: +81 561 71 7460, fax: +81 561 63 6136.
E-mail address: kudo-ken@mosk.tytlabs.co.jp (K. Kudo).

http://dx.doi.org/10.1016/j.electacta.2016.04.023
0013-4686/

induced morphological changes, and similar effects can appear also for the oxygen transport properties, too. The origins of these "thin-film effects" are not understood and the contributions of the two interfaces and polymer in-between to those effects are not clarified, either.

In this study, our previous model experiment was extended to Nafion films thinner than 100 nm, and their interfacial oxygen permeation resistances as well as the oxygen diffusion coefficient and oxygen solubility inside the bulk ionomer were measured at 313–353 K and relative humidity of 30–90%RH.

2. Experimental

For evaluating all physical properties controlling the oxygen permeation through the ionomer, two electrochemical measurements were carried out: (i) measurements on ionomer thin films and (ii) measurement on a thick ionomer film. Basic equations behind the experiments, measurements, experimental apparatus, sample preparations, detailed experimental conditions are described in this Section.

2.1. Basic equations

2.1.1. Equations used in measurements on thin films

Fig. 1 shows a schematic of a steady state oxygen concentration profile in an ionomer film on a planar Pt electrode in a low potential range, where the rate of the ORR is fully limited by the oxygen transport through the ionomer thin film. The concentration profile is assumed to be controlled by three phenomena: (i) oxygen permeation at the interface between the gas phase and ionomer phase, (ii) oxygen diffusion inside the ionomer, and (iii) oxygen permeation through the interface between the ionomer and Pt electrode. The flux of (i) is assumed to be proportional to the difference between the concentration in the ionomer at the gas interface and concentration determined by the dissolution equilibrium as follows,

$$j_{O2} = -k_{ion}(c_{eq} - c_{ion}), \tag{1}$$

where j_{O2} is the oxygen flux, k_{ion} means the apparent rate constant for the permeation at the gas/ionomer interface, c_{eq} is the equilibrium oxygen concentration and c_{ion} is the oxygen concentration at the ionomer surface. Here, c_{eq} is related to the concentration at the gas phase through the Henry's law as follows,

$$c_{eq} = K_H P_{O2}, \tag{2}$$

where K_H is Henry's constant and P_{O2} is oxygen partial pressure in the gas phase.

Similarly to Eq. (1), the flux of (iii) is described as a linear function of the difference between the concentration in the ionomer at the Pt interface (c_{Pt}) and that on the Pt surface, which equals to virtually zero at this condition, as follows,

$$j_{O2} = -k_{Pt}c_{Pt}, \tag{3}$$

where k_{Pt} indicates the apparent rate constant for the permeation at the ionomer/Pt interface.

The diffusion flux through the ionomer (ii) is, then, described by the Fick's law as follows,

$$j_{O2} = -D\frac{dc}{dx}, \tag{4}$$

where D is the oxygen diffusion coefficient of the ionomer and c is the oxygen concentration in the ionomer and x is the length in thickness direction. If D can be assumed uniform throughout the ionomer thickness,

$$j_{O2} = -D\frac{c_{ion} - c_{Pt}}{x_0}, \tag{5}$$

where x_0 is the ionomer thickness. At the steady state condition, all fluxes described by Eqs. (1), (3) and (5) are equal and related with the limiting current density (j_d) of ORR as follows,

$$j_d = -nFj_{O2}, \tag{6}$$

where n is the number of electrons involved in ORR and F is the Faraday's constant. From Eq. (6), the following equation is derived:

$$\frac{P_{O2}}{j_d} = \frac{1}{nFDK_H}x_0 + \frac{1}{nFK_H}\left(\frac{1}{k_{Pt}} + \frac{1}{k_{ion}}\right). \tag{7}$$

By using Eq. (7), the oxygen permeation resistance, R_{O2}, is described using the physical properties defined in Eqs. (1)–(6) as follows,

$$R_{O2} \equiv \frac{nFc_{gas}}{j_d} = \frac{1}{RTDK_H}x_0 + \frac{1}{RTK_H}\left(\frac{1}{k_{Pt}} + \frac{1}{k_{ion}}\right), \tag{8}$$

where c_{gas} means the oxygen concentration in gas phase, R is the gas constant and T is the temperature.

By assuming constant D and K_H independent of the film thickness x_0, the interfacial resistance $\frac{1}{K_H}\left(\frac{1}{k_{Pt}} + \frac{1}{k_{ion}}\right)$ can be separately determined as an intercept in a plot of the measured $\frac{P_{O2}}{j_d}$ versus the ionomer thickness x_0 from Eq. (7). The assumption on the constant D and K_H are still arguable because several recent experiments indicated that water uptake and proton transport properties significantly change when the film thickness was decreased to be less than 50–100 nm [30,38,40,41]. These changes were attributed to confinement effects or substrate-induced morphological changes in Nafion, and those changes may affect the oxygen solubility and diffusivity, too. The effects can be evaluated by examining the deviations of the measured data from the linear Eq. (7), and to do it, films at least thinner than 50 nm are necessary. The thinner the films are also necessary to more-

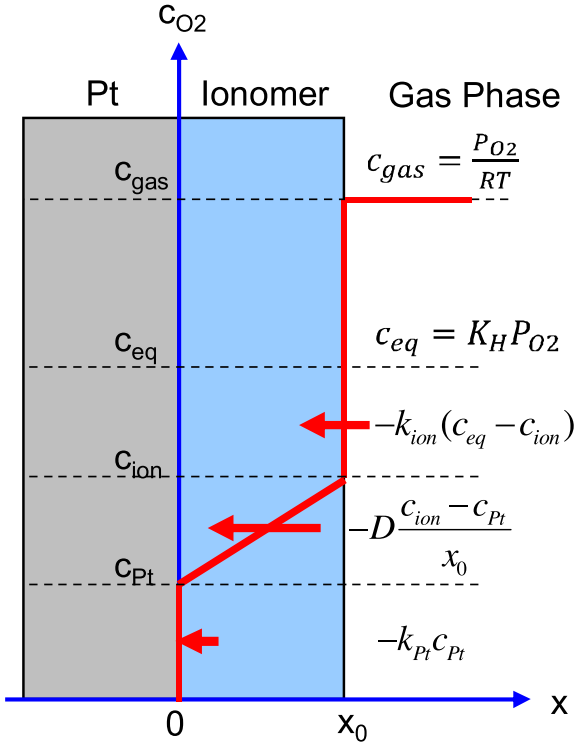

Fig. 1. Schematic of oxygen concentration profile in ionomer film.

accurately determine the apparent interfacial permeation constants k_{Pt}+k_{ion} since the intercept corresponds to the resistance at the ultimately thin ionomer film ($x_0 = 0$). As described in Section 1, our previous measurements were done on the ionomer films with a thickness of 200–800 nm, which are, however, much thicker than the ionomers (~10 nm) in the MEAs and could be too thick to examine the linearity of Eq. (7) and to determine the interfacial resistance accurately. In this study, as described in Section 2.2, an electrochemical cell for the measurements of model electrode was newly developed, and the measurements were extended to Nafion films with a thickness of 20–100 nm prepared by a method described in Section 2.3.

2.1.2. Equations used in measurements on thick films

By using Eq. (7), the non-interfacial resistivity $\frac{1}{DK_H}$ can be separately determined as a slope of Eq. (7) by using Nafion thin films with different thicknesses of x_0. This measurement, however, cannot separately evaluate the diffusion coefficient D and Henry's constant K_H (or the equilibrium concentration c_{eq}).

The separate evaluation were carried out by measuring the limiting current transition of ORR current, which flows through the interface between the Pt electrode and a Nafion thick film after the potential step measurements under O_2 atmosphere [46–57]. When the potential is stepped from 1.1 to 0.4 V (vs. RHE), for example, the transitional limiting current controlled by oxygen transport inside the thick Nafion film will be observed. By assuming that the Nafion film is thick enough to neglect effects by the interfaces, the transition of the concentration profile inside the thick Nafion film can be analytically derived, and the transitional limiting current can be described as the Cottrell-like equation [56,58] as follows,

$$I_{lim} = nF\pi r_0 D c_{eq}\left[1 + \frac{r_0}{(\pi Dt)^{1/2}} + 0.2732exp\frac{-0.3911r_0}{(Dt)^{1/2}}\right], \quad (9)$$

where I_{lim} is the limiting current, r_0 is the radius of the working electrode and t is the time passed from the potential step. D and c_{eq} in Eq. (9) can be determined by fitting this equation to the measured transitional limiting current.

It is to be noted that there are limitations to apply the data from the actual experiments to Eq. (9). Immediately after the potential step, the current generated by double-layer discharging is dominant, and therefore, the ORR current is difficult to be separated from the overall current. In contrast, after a few seconds from the potential step, the diffusion front of oxygen concentration reaches to the border of the Nafion thick film at the opposite side of the working electrode, and therefore, the assumption of the semi-infinite diffusion used to derive Eq. (9) is not satisfied in this condition.

In this study, a Nafion film with a thickness of 100 μm was prepared and used in the experiments. For this Nafion film, the data from 0 to 0.2 s and after 1.2 s were excluded from the data to determine D and c_{eq} by the fittings.

2.2. Experimental cell

Fig. 2a shows a schematic of the experimental cell. For the both measurements for thin and thick Nafion ionomers, the films were located in contact with a Pt disk working microelectrode sealed in a glass tube. The counter electrode was comprised by a platinized Pt mesh coated with Nafion and was placed below the Nafion thin film. The reference electrode was also comprised of a platinized Pt mesh coated with Nafion and was placed in another compartment supplied with humidified 2% (in dry base) H_2 gas (N_2 balance). The potential of this reference electrode was converted to the potential scaled with reversible hydrogen electrode (RHE) at 101 kPa H_2 by Nernst equation.

For the case of the Nafion thin films, as shown in Fig. 2b, a recast thin film was located in contact with a Pt mesh coated by Nafion to supply O_2 gas to the working electrode through the Pt mesh for obtaining the steady state ORR current density. In the previous experiments [18,19], for the film less than 200 nm, the I-R loss was too large for accurate analysis because the current was too large for the long and narrow proton conducting path. In the present study, to decrease the I-R loss, the working electrode was changed from a 6250 μm^2 rectangle to a 78.5 μm^2 circle by utilizing the microelectrode with a diameter of 10 μm, and this improvement has enabled accurate measurement of the limiting current density of ORR for Nafion thin films less than 100 nm.

For the case of the Nafion thick films, as shown in Fig. 2c, a recast thick film in equilibrium with the O_2 gas was located in contact with a commercial Nafion membrane, and the limiting current flows through the working electrode was measured after the potential step. With the thick film, the current density is small enough to use a larger microelectrode with a diameter of 50 μm. To certainly obtain the diffusion limited current, the working electrode of the 50 μm diameter Pt was platinized to increase the surface area.

In both experiments, the electrochemical cell was placed in a convection oven, where the temperature and relative humidity were controlled to be 313–353 K and 30–90%RH, respectively.

2.3. Sample preparations

Nafion thin films with various thicknesses were prepared on the working electrodes from 0.3–0.7 wt. % Nafion solutions (DE2020, DuPont) diluted by 1-propanol by a solution casting technique. After drying them at room temperature, they were annealed at 403 K for an hour. The thickness of the Nafion thin films on the working electrode was measured by using a surface profile measuring system (DEKTAK^3, Veeco Instruments) under a N_2 flow condition by scratching the films after the electrochemical measurement.

A Nafion thick film with the thickness of 100 μm under the humidified condition was prepared by casting the Nafion solution on a petri dish and was annealed at 403 K for an hour after drying the film at room temperature similarly to the case of the thin film. The fabricated thick film was sequentially soaked in 3% H_2O_2 aqueous solution, Millipore ultrapure water, 2 mol dm^{-3} HNO_3 and the ultrapure water in this order at 353 K for an hour each to clean it. The thickness of the film was controlled to be approximately 100 μm at humidified conditions.

2.4. Detailed experimental procedures

For the case of the measurements on the Nafion thin films, the limiting current density, j_d, was measured by sweeping the potential from 0.1 V to 1.1 V with 0.1 V s^{-1} under oxygen concentrations of 0 (N_2), 0.1 or 1% (N_2 balance) at 313 K, 333 K and 353 K, and at 30, 60 and 90%RH.

For the case of the measurements on the Nafion thick films, the transitional limiting current was measured after stepping the potential from 1.1 to 0.4 V vs. RHE. Temperature and relative humidity were controlled similarly to the case of the measurements on the Nafion thin films.

3. Results and Discussion

3.1. Oxygen transport resistance obtained from thin Nafion films

Diffusion controlled current densities, j_d, were determined by cyclic voltammetry using the 10 μm diameter Pt microelectrodes

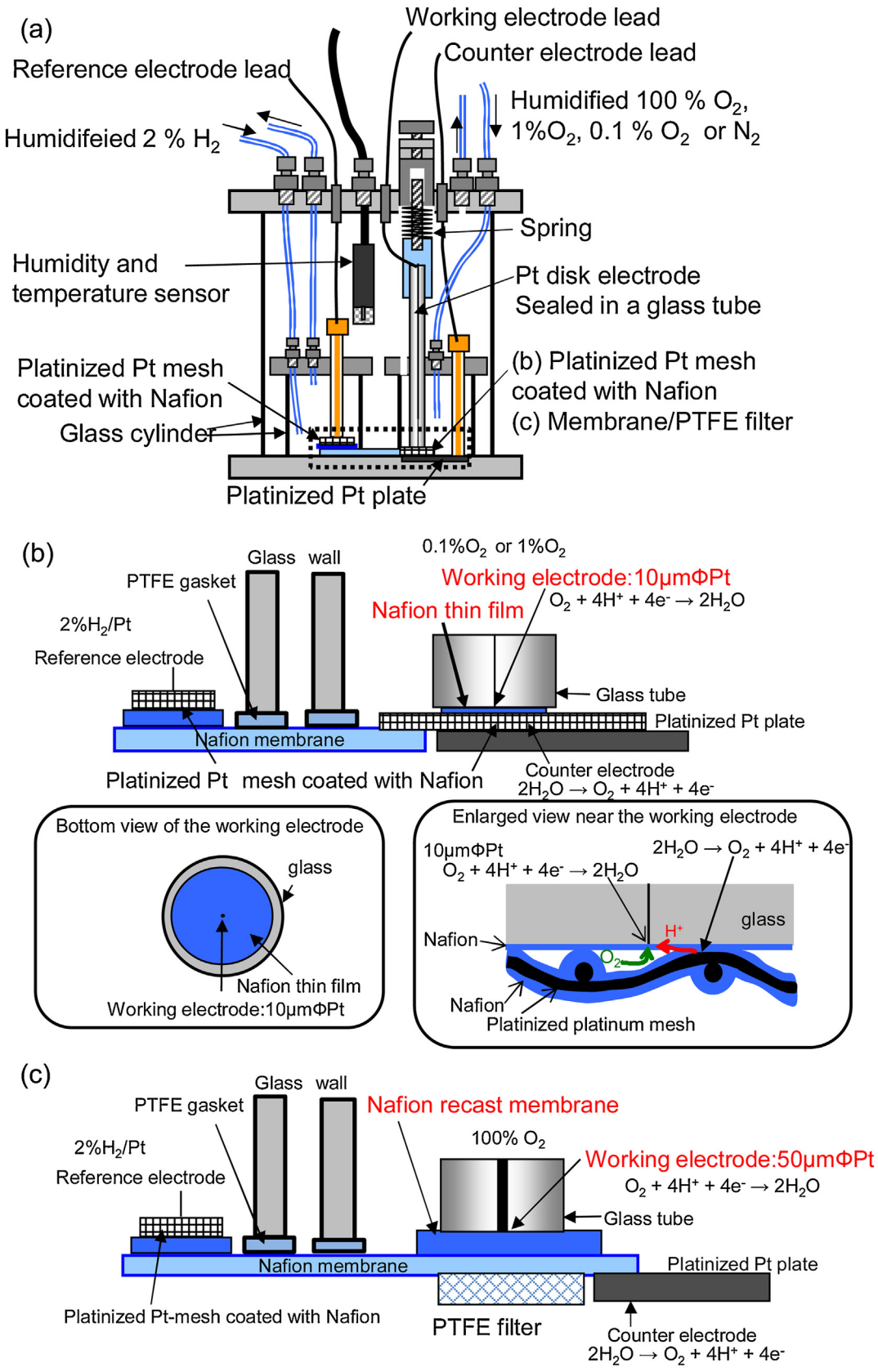

Fig. 2. Schematic of the cell used to measure oxygen transport properties. (a) Arrangement of the vessels, sensor and electrodes. (b) (c) Arrangement of electrodes and samples surrounded by the dotted lines in (a) for thin film(b) and thick film(c).

coated by the Nafion thin films with thicknesses of 20–100 nm. Fig. 3 (a) shows cyclic voltammograms (CVs) of the Pt for a Nafion film with a thickness of 39 nm measured under N_2 and 0.1% O_2, and Fig. 3 (b) shows CVs measured under N_2 and 1% O_2. Temperature and relative humidity were controlled at 313 K and 60%RH, respectively, in those measurements. In the CVs (red lines) under the N_2 atmosphere shown in both Fig. 3 (a) and (b), hydrogen adsorption/desorption currents and Pt oxidation/reduction currents are observed below 0.4 V and above 0.7 V, respectively. Under O_2 containing atmospheres, as shown by blue lines, negative (reduction) currents flow below 0.8 V. These additional currents correspond to oxygen reduction currents, and therefore, the ORR currents can be determined by subtracting the current under the N_2 atmosphere from those under the O_2 atmospheres, as shown by black lines in Figs. 3 (a) and (b). The ORR currents increase when the electrode potential is decreased from 0.80 V and reach maxima around 0.25 V. Unlike usual CVs of the ORR measured on Pt electrodes in past studies, clear plateaus do not appear in the measured voltammograms. It should be also mentioned that the currents linearly increases with the increase in the oxygen partial pressure. This result indicates that the increase in the current density from 0.80 V to 0.25 V is dominated by non-ohmic resistances. The observed potential-dependences in the measured currents are explained reasonably by adsorbate-induced potential-dependent oxygen diffusion resistances suggested by Ono et al. [12]. With the decrease in the electrode potential from 0.80 to 0.25 V, for example, the surface coverage of (hydr)oxides and sulfonic acid groups adsorbed on the Pt electrode decrease, and this results in the increase in the active surface domains for the ORR. The increase in the active domains can enlarge the oxygen diffusion paths from the Nafion to the electrode surface and can contribute on the decrease in the oxygen diffusion resistance if the length-scale of the active domains is comparable to the length-scale of the oxygen diffusion resistance layers. An opposite thing can occur at the potential below 0.25 V, where the adsorbed hydrogen atoms can narrow the oxygen diffusion paths. On the basis of the mechanism described above, the effects by the specifically adsorbed species are judged to be smallest around 0.25 V, and the currents at this potential were used as the diffusion limiting currents in this study. In addition, it should be noted that at this low potential, 2-electron ORR pathway forming H_2O_2 can contribute on the overall currents, but the effects were judged to be negligibly small (less than 5%) as reported by Ohma et al. [59].

The j_d can be obtained by dividing I_d by the electrode area, then $\frac{P_{O2}}{j_d}$ in Eq. (7) can be calculated. The obtained $\frac{P_{O2}}{j_d}$ under 0.1% O_2 and 1% O_2 were 40.7 $A^{-1}\cdot m^2\cdot Pa$ and 41.2 $A^{-1}\,m^2\,Pa$, respectively. This result of constant $\frac{P_{O2}}{j_d}$ over a wide range of current density, which means that the j_d is linearly proportional to the P_{O2}, indicates that the experimental set-up successfully eliminated undesired effects by I-R losses in the electrochemical cell and flooding of the working electrode by generated waters. It should be, however, noted that when the film thickness was less than 30 nm under 30% RH and 1% O_2, where large ORR currents flow through highly resistant films, I-R losses were too large to obtain consistent diffusion-limiting current. Those data were, therefore, excluded from the discussion described later in this article. In addition, the effects of water and heat generations are most likely negligible because of the large electrode including a grass region and small current.

Fig. 4 shows the relation between the measured $\frac{P_{O2}}{j_d}$ and film thickness measured at 313–353 K and 30-90%RH, which indicates that $\frac{P_{O2}}{j_d}$ linearly increases with the film thickness, x_0, as expected from Eq. (7). While the error of the interfacial resistance in the previous study was in the range from 13 to 82 $A^{-1}\,m^2\,Pa$ at 353 K and 60%RH, that in the present study is in the range from 6.5 to 11.6 $A^{-1}\,m^2\,Pa$ at 353 K and 60%RH, which is obtained from a 95% confidence interval of the intercept value as shown in Fig. 4(c'). The improved error of the present study within ca 5 $A^{-1}\,m^2\,Pa$ was achieved through the measurement of $\frac{P_{O2}}{j_d}$ for much thinner films.

The interfacial resistances, $\frac{1}{K_H}\left(\frac{1}{k_{Pt}}+\frac{1}{k_{ion}}\right)$, obtained from the intercepts of the linear plots at 313–353 K shown in Fig. 4 are shown as functions of the relative humidity in Fig. 5(a). Similarly, the oxygen transport resistivities, $\frac{1}{DK_H}$, inside the thin films obtained from the slopes of the linear plots in Fig. 4 are summarized in Fig. 5(b) as functions of the relative humidity. Both the interfacial resistance and non-interfacial resistivity decrease with the increase in the relative humidity.

3.2. Oxygen diffusion coefficient and solubility obtained from thick Nafion film

The oxygen diffusion coefficient, D, and the Henry's constant, K_H, (or solubility), were separately determined by measuring the transitional diffusion-limiting current densities after the potential steps on the Pt microelectrode on the Nafion thick film as described in Section 2.1.2. Similarly to the measurements on the Nafion thin films shown in Section 3.1, the measurements on the thick Nafion film were executed under N_2 atmosphere and O_2 atmosphere while 100% O_2 was used for this measurement. The measured reduction currents at 353 K and 60%RH are shown as functions of $t^{-1/2}$ in Fig. 6. The transitional reduction current under N_2 atmosphere shown in the red line in Fig. 6 is the current by the reduction of Pt oxides. Therefore, the diffusion limited ORR, $-I_{lim}$, (black line) was

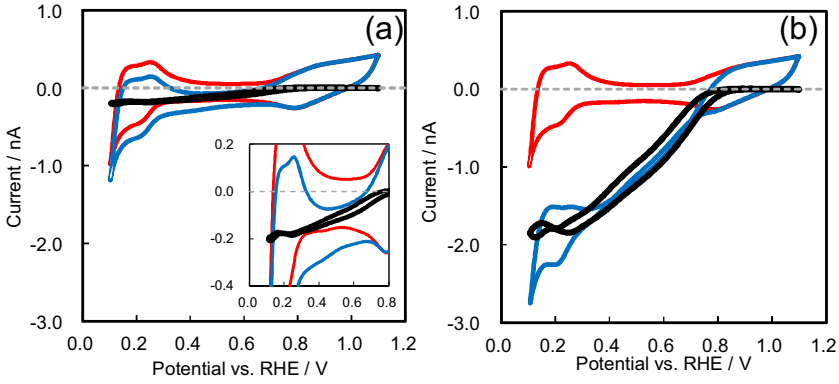

Fig. 3. Cyclic voltammograms of the Pt with 39 nm-thick film under N_2(red), (a) 0.1% O_2 (blue), (b) 1% O_2 (blue) and subtract current in N_2 from current in O_2 (black) at 313 K and 60%RH. Inset in (a) is enlarged view of the subtracted current. (For interpretation of the references to color in this figure legend and text, the reader is referred to the web version of this article.)

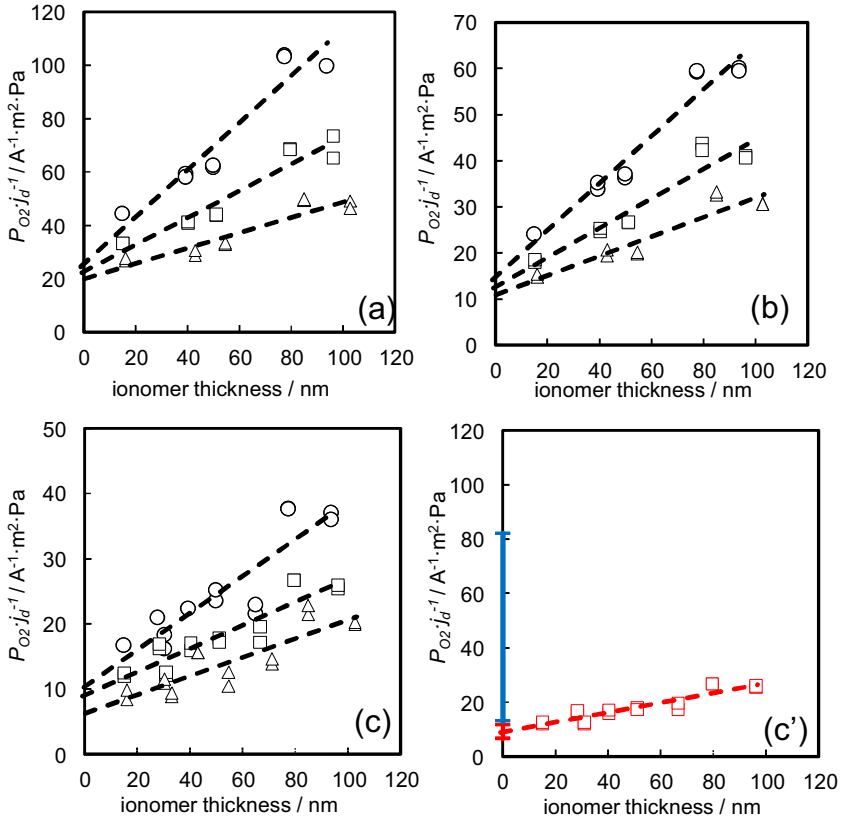

Fig. 4. Relation between P_{O2}/i_d and film thickness at 30%RH (circle), 60%RH (square), 90%RH (triangle), 313 K (a), 333 K (b) 353 K (c). (c'): 95% confidence interval of the intercept at 353 K and 60%RH in the present study(red bar) and error of the previous study [18] (blue bar). (For interpretation of the references to color in this figure legend, the reader is referred to the web version of this article.)

obtained by subtracting the Pt oxide reduction current from the reduction current under O_2 atmosphere (blue line) and, then, D and K_H were calculated.

Fig. 7(a), (b) and (c) show D, K_H and DK_H, respectively, obtained by the fittings as functions of the relative humidity. D increases with the increase in the relative humidity while K_H decreases with the increase in the relative humidity. Since D changes more sensitively to the relative humidity, the non-interfacial permeability term, DK_H, increases with the increase in the relative humidity and therefore, oxygen transport resistivity, $\frac{1}{DK_H}$, inside the Nafion film decreases with the increase in the relative humidity. The obtained humidity-dependences of the oxygen transport properties are consistent also with the oxygen transport properties under dry and fully humidified conditions reported in the previous studies [51,55,60] as shown in Fig. 7.

It should be noted that the resistivity obtained by the measurements on the thick films are consistent with those obtained by the measurements on the thin films as shown in Fig. 8. The agreements indicate that the non-interfacial oxygen transport resistivity inside the Nafion films is not significantly different even when the film thickness is tens of nm. This result is also consistent with the result reported by Liu et al. [45], who reported that the non-interfacial oxygen transport resistivity is constant up to the film thickness of 50 nm.

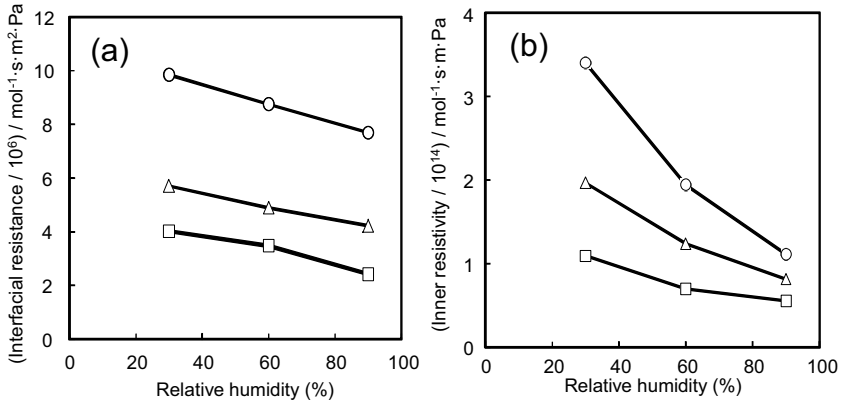

Fig. 5. Humidity dependence of (a): interfacial resistance and (b): inner oxygen transport resistivity of Nafion thin film at 313 K (circle), 333 K (triangle) and 353 K (square).

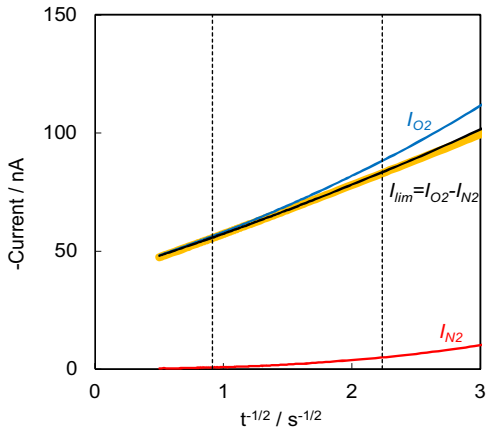

Fig. 6. Relation between currents and $t^{-1/2}$ at 353 K and 60%RH under N_2 (red), O_2 (blue), subtracted current (black) and fitting result (yellow). Dotted lines show fitting range of the subtracted current. (For interpretation of the references to color in this figure legend and text, the reader is referred to the web version of this article.)

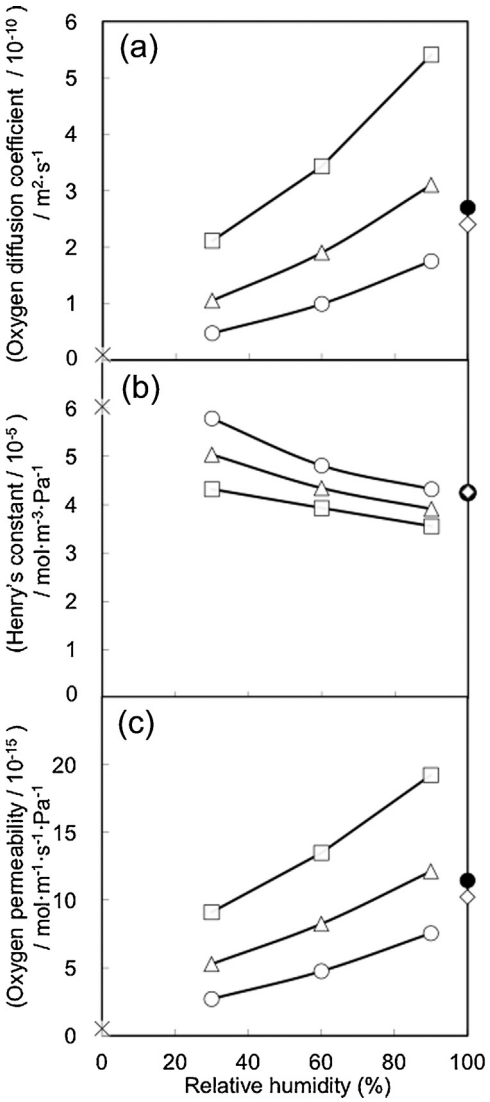

Fig. 7. Humidity dependence of (a): oxygen diffusion coefficient, (b): Henry's constant of oxygen and (c): oxygen permeability in Nafion thick film at 313 K (open circle), 333 K (triangle) and 353 K (square). Nafion 117 at 303 K under dry condition [60] (cross), Nafion 117 at 323 K and 100%RH (diamond) [51], recast Nafion at 313 K and 100%RH (closed circle) [55].

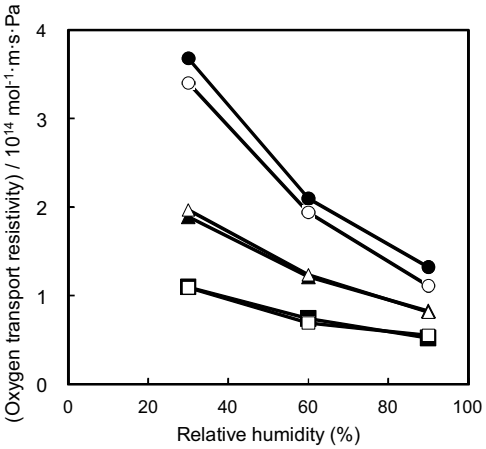

Fig. 8. Humidity dependence of oxygen transport resistivity of Nafion thick film from Fig. 7(c) (closed) and Nafion thin film from Fig. 5(b) (open) at 313 K (circle), 333 K (triangle) and 353 K (square).

3.3. Rate limiting process of oxygen permeation

By dividing the obtained interfacial resistance by the inner resistivity, equivalent thickness of the interfacial resistance against the inner resistivity is calculated as shown in Fig. 9, calculated equivalent thicknesses are 30–70 nm, which are much thicker than a typical ionomer thickness of ~10 nm observed in MEAs. The result indicates that the oxygen permeation fluxes through the ionomers in MEAs are dominantly controlled by the interfacial oxygen permeation.

The interfacial resistance measured at 353 K agree well with the reported resistance values from the voltage drops measured in the MEAs at 353 K as shown in Fig. 10 and, therefore, it is safely concluded that the interfacial oxygen transport resistance is the dominant factor for the voltage drops in the high current density regions observed in the MEAs in the past literatures [12,14]. The conclusion is consistent with that given by Greszler et al. [14], who thought that the observed voltage drops could not be explained by the oxygen permeation resistances estimated from properties of either the bulk Nafion or the carbon agglomerates in the catalyst layers.

The results given by the model experiments are also consistent with our recent theoretical results obtained by molecular dynamics techniques [21]. In the theoretical study, steady-state oxygen permeations were simulated at interfaces between bare Pt (111) and Nafion thin films with a thickness of 2–4 nm, and the

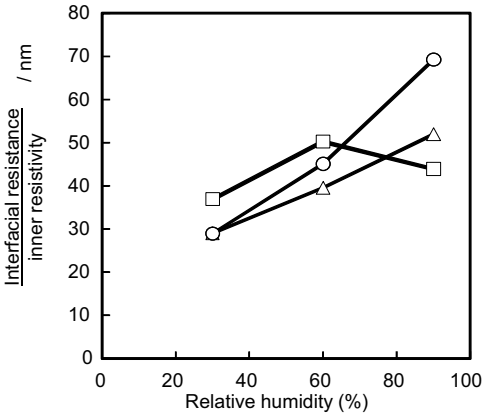

Fig. 9. Equivalent thickness of Nafion film to interfacial oxygen transport resistance at 313 K (circle), 333 K (triangle) and 353 K (square).

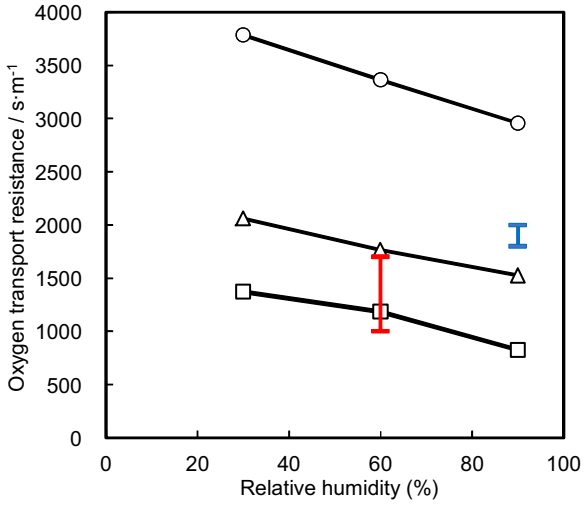

Fig. 10. Interfacial resistance of Nafion thin film obtained from model electrode (black) at 313 K (circle), 333 K (triangle) and 353 K (square). Bars represent interfacial resistance obtained from MEA experiment and numerical model at 353 K. (red: Greszler et al. [14], blue: Ono et al. [12]). (For interpretation of the references to color in this figure legend, the reader is referred to the web version of this article.)

calculated permeation fluxes were converted to the diffusion limiting current densities. Although the theory simplified the complex polycrystalline electrode morphology by the single crystal surface and neglected the effects by the adsorbates, the model reasonably described the O_2 permeation through the Nafion thin film coated on the bare Pt surface and gave the limiting current density close to the experimental results reported in this study. Detailed theoretical analysis indicated that the overall oxygen permeation are limited by energetic barriers of 10-20 kJ·mol^{-1} at the ionomer/Pt interface. The sources of the high interfacial energetic barriers at the ionomer/Pt interface were shown to be dense ionomer layers formed near the Pt surfaces. Therefore, this resistance is not, strictly speaking, interfacial. From an experimental point of view, however, it seems "interfacial" because it is obtained by interpolating the experimental data to zero thickness. In this paper, therefore, we use the term "interfacial resistance at the Pt/ionomer" in the latter broader sense. The theoretical results indicate that the interfacial oxygen permeations is not inhibited by absorbed water molecules but by polymers and

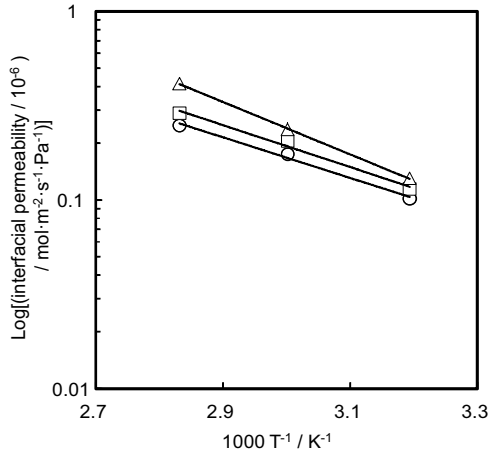

Fig. 11. Temperature dependence of interfacial permeability for Nafion thin film on Pt.

that indication qualitatively explains why the interfacial resistance does not increase with the increase in the relative humidity.

The presence of the energetic barriers also qualitatively explains the Arrhenius-type temperature-dependence of the interfacial oxygen permeation rate, $K_H \frac{k_{Pt} k_{ion}}{k_{Pt}+k_{ion}}$, summarized in Fig. 11. The apparent activation energy of the interfacial permeation rate is 21–27 kJ mol^{-1}, which is close to the energetic barriers obtained by molecular dynamics techniques [21].

The discussion above suggests that the original model of Fig. 1, strictly speaking, needs to be modified since the model assumes a uniform diffusion constant D throughout the film while the presence of high-energy-barrier layer means that D in the layer is much smaller. However, the overall analytical process, in which the total resistance was separated to the resistance that is not dependent on the film thickness and the resistance that is, can be regarded still valid and modification of the model is not practically necessary.

4. Conclusions

The oxygen transport resistances of the Nafion thin films less than 100 nm and of the Nafion thick film were evaluated to clarify the dominant part of the oxygen transport loss in the ionomer for the cathode catalyst layer of PEFCs. The interfacial oxygen transport resistance and inner resistivity of the Nafion thin film were separately determined by the relation between P_{O2}/j_d and the film thickness. The equivalent thickness of the interfacial resistance against the inner resistivity is 30–70 nm, which is much thicker than a typical ionomer thickness of ~10 nm observed in MEAs. The interfacial resistance measured by the model electrode is consistent with the previous literatures measured in MEAs. From the above results and our recent theoretical results, it is concluded that the oxygen permeation fluxes through the ionomers in MEAs are dominantly controlled by the oxygen permeation at the Pt/ionomer interface.

References

[1] D. Papageorgopoulos, Annual Merit Review Proceedings Fuel Cell 2013 (2013).
[2] V. Stamenkovic, B.S. Mun, K.J. Mayrhofer, P.N. Ross, N.M. Markovic, J. Rossmeisl, J. Greeley, J.K. Norskov, Changing the activity of electrocatalysts for oxygen reduction by tuning the surface electronic structure, Angewandte Chemie 45 (2006) 2897–2901.
[3] P. Strasser, S. Koh, T. Anniyev, J. Greeley, K. More, C. Yu, Z. Liu, S. Kaya, D. Nordlund, H. Ogasawara, M.F. Toney, A. Nilsson, Lattice-strain control of the activity in dealloyed core-shell fuel cell catalysts, Nature chemistry 2 (2010) 454–460.
[4] C.H. Cui, L. Gan, H.H. Li, S.H. Yu, M. Heggen, P. Strasser, Octahedral PtNi Nanoparticle Catalysts: Exceptional Oxygen Reduction Activity by Tuning the Alloy Particle Surface Composition, Nano letters 12 (2012) 5885–5889.
[5] D.F. van der Vliet, C. Wang, D. Tripkovic, D. Strmcnik, X.F. Zhang, M.K. Debe, R.T. Atanasoski, N.M. Markovic, V.R. Stamenkovic, Mesostructured thin films as electrocatalysts with tunable composition and surface morphology, Nature materials 11 (2012) 1051–1058.
[6] E. Toyoda, R. Jinnouchi, T. Ohsuna, T. Hatanaka, T. Aizawa, S. Otani, Y. Kido, Y. Morimoto, Catalytic Activity of Pt/TaB2(0001) for the Oxygen Reduction Reaction, Angew. Chem. –Int. Edit. 52 (2013) 4137–4140.
[7] C. Chen, Y.J. Kang, Z.Y. Huo, Z.W. Zhu, W.Y. Huang, H.L.L. Xin, J.D. Snyder, D.G. Li, J.A. Herron, M. Mavrikakis, M.F. Chi, K.L. More, Y.D. Li, N.M. Markovic, G.A. Somorjai, P.D. Yang, V.R. Stamenkovic, Highly Crystalline Multimetallic Nanoframes with Three-Dimensional Electrocatalytic Surfaces, Science 343 (2014) 1339–1343.
[8] P. Hernandez-Fernandez, F. Masini, D.N. McCarthy, C.E. Strebel, D. Friebel, D. Deiana, P. Malacrida, A. Nierhoff, A. Bodin, A.M. Wise, J.H. Nielsen, T.W. Hansen, A. Nilsson, I.E.L. Stephens, I. Chorkendorff, Mass-selected nanoparticles of PtxY as model catalysts for oxygen electroreduction, Nature chemistry 6 (2014) 732–738.
[9] X.Q. Huang, Z.P. Zhao, L. Cao, Y. Chen, E.B. Zhu, Z.Y. Lin, M.F. Li, A.M. Yan, A. Zettl, Y.M. Wang, X.F. Duan, T. Mueller, Y. Huang, High-performance transition metal-doped Pt3Ni octahedra for oxygen reduction reaction, Science 348 (2015) 1230–1234.
[10] T. Mashio, A. Ohma, K. Shinorara, Advanced In-situ Analysis of Reactant Gas Partial Pressure at Catalyst Layer/PEM Interfaces, ECS Transactions 16 (2008) 1009–1018.

[11] K. Sakai, K. Sato, T. Mashio, A. Ohma, K. Yamaguchi, K. Shinohara, Analysis of Reactant Gas Transport in Catalyst Layers; Effect of Pt-loadings, ECS Transactions 25 (2009) 1193–1201.
[12] Y. Ono, T. Mashio, S. Takaichi, A. Ohma, H. Kanesaka, K. Shinohara, The analysis of performance loss with low platinum loaded cathode catalyst layers, ECS Transactions 28 (2010) 69–78.
[13] N. Nonoyama, S. Okazaki, A.Z. Weber, Y. Ikogi, T. Yoshida, Analysis of Oxygen-Transport Diffusion Resistance in Proton-Exchange-Membrane Fuel Cells, Journal of The Electrochemical Society 158 (2011) B416.
[14] T.A. Greszler, D. Caulk, P. Sinha, The Impact of Platinum Loading on Oxygen Transport Resistance, Journal of the Electrochemical Society 159 (2012) F831–F840.
[15] S. Jomori, K. Komatsubara, N. Nonoyama, M. Kato, T. Yoshida, An Experimental Study of the Effects of Operational History on Activity Changes in a PEMFC, Journal of the Electrochemical Society 160 (2013) F1067–F1073.
[16] Y. Ono, A. Ohma, K. Shinohara, K. Fushinobu, Influence of Equivalent Weight of Ionomer on Local Oxygen Transport Resistance in Cathode Catalyst Layers, Journal of the Electrochemical Society 160 (2013) F779–F787.
[17] A.Z. Weber, A. Kusoglu, Unexplained transport resistances for low-loaded fuel-cell catalyst layers, J. Mater. Chem. A 2 (2014) 17207–17211.
[18] K. Kudo, T. Suzuki, Y. Morimoto, Analysis of Oxygen Dissolution Rate from Gas Phase into Nafion Surface and Development of an Agglomerate Model, ECS Transactions 33 (2010) 1495–1502.
[19] T. Suzuki, K. Kudo, Y. Morimoto, Model for investigation of oxygen transport limitation in a polymer electrolyte fuel cell, Journal of Power Sources 222 (2013) 379–389.
[20] K. Kudo, Y. Morimoto, Analysis of Oxygen Transport Resistance of Nafion thin film on Pt electrode, ECS Transactions 50 (2012) 1487–1494.
[21] R. Jinnouchi, K. Kudo, N. Kitano, Y. Morimoto, Molecular Dynamics Simulations on O2 Permeation through Nafion Ionomer on Platinum Surface, Electrochimica Acta 188 (2016) 767–776.
[22] Z. Siroma, R. Kakitsubo, N. Fujiwara, T. Ioroi, S.-i. Yamazaki, K. Yasuda, Depression of proton conductivity in recast Nafion® film measured on flat substrate, Journal of Power Sources 189 (2009) 994–998.
[23] T. Mashio, K. Malek, M. Eikerling, A. Ohma, H. Kanesaka, K. Shinohara, Molecular Dynamics Study of Ionomer and Water Adsorption at Carbon Support Materials, J. Phys. Chem. C 114 (2010) 13739–13745.
[24] M. Bass, A. Berman, A. Singh, O. Konovalov, V. Freger, Surface-Induced Micelle Orientation in Nafion Films, Macromolecules 44 (2011) 2893–2899.
[25] R. Koestner, Y. Roiter, I. Kozhinova, S. Minko, AFM imaging of adsorbed Nafion polymer on mica and graphite at molecular level, Langmuir: the ACS journal of surfaces and colloids 27 (2011) 10157–10166.
[26] R. Koestner, Y. Roiter, I. Kozhinova, S. Minko, Effect of Local Charge Distribution on Graphite Surface on Nafion Polymer Adsorption as Visualized at the Molecular Level, The Journal of Physical Chemistry C 115 (2011) 16019–16026.
[27] A. Kongkanand, Interfacial Water Transport Measurements in Nafion Thin Films Using a Quartz-Crystal Microbalance, The Journal of Physical Chemistry C 115 (2011) 11318–11325.
[28] D.K. Paul, A. Fraser, K. Karan, Towards the understanding of proton conduction mechanism in PEMFC catalyst layer: Conductivity of adsorbed Nafion films, Electrochemistry Communications 13 (2011) 774–777.
[29] S.K. Dishari, M.A. Hickner, Antiplasticization and Water Uptake of Nafion Thin Films, ACS Macro Letters 1 (2012) 291–295.
[30] S.A. Eastman, S. Kim, K.A. Page, B.W. Rowe, S.H. Kang, S.C. DeCaluwe, J.A. Dura, C.L. Soles, K.G. Yager, Effect of Confinement on Structure, Water Solubility, and Water Transport in Nafion Thin Films, Macromolecules 45 (2012) 7920–7930.
[31] M.A. Modestino, A. Kusoglu, A. Hexemer, A.Z. Weber, R.A. Segalman, Controlling Nafion Structure and Properties via Wetting Interactions, Macromolecules 45 (2012) 4681–4688.
[32] G.C. Abuin, M.C. Fuertes, H.R. Corti, Substrate effect on the swelling and water sorption of Nafion nanomembranes, J. Membr. Sci. 428 (2013) 507–515.
[33] S.K. Dishari, M.A. Hickner, Confinement and Proton Transfer in NAFION Thin Films, Macromolecules 46 (2013) 413–421.
[34] S. Kim, J.A. Dura, K.A. Page, B.W. Rowe, K.G. Yager, H.J. Lee, C.L. Soles, Surface-Induced Nanostructure and Water Transport of Thin Proton-Conducting Polymer Films, Macromolecules 46 (2013) 5630–5637.
[35] M.A. Modestino, D.K. Paul, S. Dishari, S.A. Petrina, F.I. Allen, M.A. Hickner, K. Karan, R.A. Segalman, A.Z. Weber, Self-Assembly and Transport Limitations in Confined Nafion Films, Macromolecules 46 (2013) 867–873.
[36] H.F.M. Mohamed, S. Kuroda, Y. Kobayashi, N. Oshima, R. Suzuki, A. Ohira, Possible presence of hydrophilic SO3H nanoclusters on the surface of dry ultrathin Nafion (R) films: a positron annihilation study, Physical Chemistry Chemical Physics 15 (2013) 1518–1525.
[37] J.R. O'Dea, N.J. Economou, S.K. Buratto, Surface Morphology of Nafion at Hydrated and Dehydrated Conditions, Macromolecules 46 (2013) 2267–2274.
[38] D.K. Paul, K. Karan, A. Docoslis, J.B. Giorgi, J. Pearce, Characteristics of Self-Assembled Ultrathin Nafion Films, Macromolecules 46 (2013) 3461–3475.
[39] S.C. DeCaluwe, P.A. Kienzle, P. Bhargava, A.M. Baker, J.A. Dura, Phase segregation of sulfonate groups in Nafion interface lamellae, quantified via neutron reflectometry fitting techniques for multi-layered structures, Soft Matter 10 (2014) 5763–5776.
[40] A. Kusoglu, D. Kushner, D.K. Paul, K. Karan, M.A. Hickner, A.Z. Weber, Impact of Substrate and Processing on Confinement of Nafion Thin Films, Advanced Functional Materials 24 (2014) 4763–4774.
[41] D.K. Paul, K. Karan, Conductivity and Wettability Changes of Ultrathin Nafion Films Subjected to Thermal Annealing and Liquid Water Exposure, The Journal of Physical Chemistry C 118 (2014) 1828–1835.
[42] D.D. Borges, G. Gebel, A.A. Franco, K. Malek, S. Mossa, Morphology of Supported Polymer Electrolyte Ultrathin Films: A Numerical Study, J. Phys. Chem. C 119 (2015) 1201–1216.
[43] Y. Guo, Y. Ono, Y. Nagao, Modification for Uniform Surface of Nafion Ultrathin Film Deposited by Inkjet Printing, Langmuir: the ACS journal of surfaces and colloids 31 (2015) 10137–10144.
[44] W.P. Kalisvaart, H. Fritzsche, W. Merida, Water Uptake and Swelling Hysteresis in a Nafion Thin Film Measured with Neutron Reflectometry, Langmuir: the ACS journal of surfaces and colloids 31 (2015) 5416–5422.
[45] H. Liu, W.K. Epting, S. Litster, Gas Transport Resistance in Polymer Electrolyte Thin Films on Oxygen Reduction Reaction Catalysts, Langmuir: the ACS journal of surfaces and colloids 31 (2015) 9853–9858.
[46] F.N. Buchi, M. Wakizoe, S. Srinivasan, Microelectrode investigation of oxygen permeation in perfluorinated proton exchange membranes with different equivalent weights, Journal of the Electrochemical Society 143 (1996) 927–932.
[47] Y. Takamura, E. Nakashima, H. Yamada, A. Tasaka, M. Inaba, Effects of Temperature and Relative Humidity on Oxygen Permeation in Nafion (R) and Sulfonated Poly(Arylene Ether Sulfone), ECS Transactions 16 (2008) 881–889.
[48] K. Ota, Y. Inoue, N. Motohira, N. Kamiya, Hydrogen oxidation and oxygen reduction at Pt microelectrode on polymer electrolytes, Journal of New Materials for Electrochemical Systems 3 (2000) 193–198.
[49] A. Parthasarathy, C.R. Martin, S. Srinivasan, INVESTIGATIONS OF THE O-2 REDUCTION REACTION AT THE PLATINUM NAFION INTERFACE USING A SOLID-STATE ELECTROCHEMICAL-CELL, Journal of the Electrochemical Society 138 (1991) 916–921.
[50] A. Parthasarathy, S. Srinivasan, A.J. Appleby, C.R. Martin, TEMPERATURE-DEPENDENCE OF THE ELECTRODE-KINETICS OF OXYGEN REDUCTION AT THE PLATINUM NAFION(R) INTERFACE—A MICROELECTRODE INVESTIGATION, Journal of the Electrochemical Society 139 (1992) 2530–2537.
[51] A. Parthasarathy, S. Srinivasan, A.J. Appleby, C.R. Martin, PRESSURE-DEPENDENCE OF THE OXYGEN REDUCTION REACTION AT THE PLATINUM MICROELECTRODE NAFION INTERFACE—ELECTRODE-KINETICS AND MASS-TRANSPORT, Journal of the Electrochemical Society 139 (1992) 2856–2862.
[52] L. Zhang, C.S. Ma, S. Mukerjee, Oxygen reduction and transport characteristics at a platinum and alternative proton conducting membrane interface, Journal of Electroanalytical Chemistry 568 (2004) 273–291.
[53] L. Zhang, C.S. Ma, S. Mukerjee, Oxygen permeation studies on alternative proton exchange membranes designed for elevated temperature operation, Electrochimica Acta 48 (2003) 1845–1859.
[54] L. Zhang, C. Hampel, S. Mukerjee, Effect of Copolymer Composition on the Oxygen Transport Properties of Sulfonated Poly(arylene ether sulfone) and Sulfonated Poly(sulfide sulfone) PEMs, Journal of The Electrochemical Society 152 (2005) A1208.
[55] K. Lee, A. Ishihara, S. Mitsushima, N. Kamiya, K.-i. Ota, Effect of Recast Temperature on Diffusion and Dissolution of Oxygen and Morphological Properties in Recast Nafion, Journal of The Electrochemical Society 151 (2004) A639.
[56] S. Mitsushima, N. Araki, N. Kamiya, K.-i. Ota, Analysis of Oxygen Reduction on Pt Microelectrode with Polymer Electrolytes of Various Exchange Capacities, Journal of The Electrochemical Society 149 (2002) A1370.
[57] D. Novitski, S. Holdcroft, Determination of O2 Mass Transport at the Pt | PFSA Ionomer Interface under Reduced Relative Humidity, ACS applied materials & interfaces 7 (2015) 27314–27323.
[58] H. Ikeuchi, M. Sato, G.P. Sato, EXPERIMENTAL-VERIFICATION OF AN EQUATION OF DIFFUSION CURRENT AT AN UNSHIELDED STATIONARY DISK ELECTRODE, Journal of Electroanalytical Chemistry 162 (1984) 321–326.
[59] A. Ohma, K. Fushinobu, K. Okazaki, Influence of Nafion® film on oxygen reduction reaction and hydrogen peroxide formation on Pt electrode for proton exchange membrane fuel cell, Electrochimica Acta 55 (2010) 8829–8838.
[60] T. Sakai, H. Takenaka, E. Torikai, GAS-DIFFUSION IN THE DRIED AND HYDRATED NAFIONS, Journal of the Electrochemical Society 133 (1986) 88–92.